Nuclear Instruments and Methods in Physics Research B 536 (2023) 119–125

Contents lists available at ScienceDirect

Nuclear Inst. and Methods in Physics Research, B

journal homepage: www.elsevier.com/locate/nimb

Statistical nature of secondary electron emission

D.M. Newson, R. Kadokura, S.J. Brawley, M. Shipman, G. Laricchia *

UCL Department of Physics and Astronomy, University College London, Gower Street, London WC1E 6BT, United Kingdom

ARTICLE INFO

Keywords:
Secondary electron
Energy-dependence
Statistical description
Log-normal

ABSTRACT

The energy-dependence of the secondary electron yield by electron impact on clean materials is shown, through comparisons with both experimental data and previous semi-empirical models, to be described well by a log-normal distribution. The maximum yield and corresponding energy are calculated in terms of the fit parameters. The function also agrees with the 'universal curve' obtained by expressing the experimental data in terms of the position and magnitude of maximum yield. The positron- and ion-induced secondary electron yields also exhibit a log-normal dependence and this is used to extend their energy ranges without prior knowledge of the position and magnitude of their maxima. In addition to their intrinsic usefulness, the results provide further support for the statistical description of inelastic processes advanced by Laricchia et al. (2018).

1. Introduction

Secondary electron (SE) emission is the excitation of a valence or core electron by an incident (primary) particle such that the excited electron is ejected from the surface of the material, typically associated with a kinetic energy ≤ 50 eV [1]. The SE yield or coefficient, denoted $\delta(E_0)$, is the number of SEs produced per incident projectile as a function of the primary kinetic energy (E_0) and is relevant to a wide-range of applications including scanning electron microscopes [1], particle accelerators [2,3], fusion apparatus [4], satellite systems [5] and extreme ultraviolet lithography [6].

Experimental studies over the last 100+ years have targeted a range of elements, compounds and materials with little consensus achieved among the results obtained, as seen in the data collated by Joy [18]. As a case in point, measurements [2,7–13] of $\delta(E_0)$ from copper are displayed in Fig. 1, illustrating their spread. All datasets show a similar form, a rapid increase with energy followed by a steady decline, but the position and magnitude of the peak varies, with lower maxima occurring at higher energies for the clean samples of Bruining & De Boer [7], Bronstein & Fraiman [8], Shimizu [9], Walker et al. [12] and Gonzalez et al. [13]. A similar behaviour can be seen, for example, in the case of platinum but not for carbon, both considered by Tolias [4]. Thus for a given material, evaluation of the SE yield at a particular impact energy from experimental results is subject to significant uncertainty.

A number of semi-empirical models have been developed to describe the energy-dependence of the SE yield in terms of a small number of material-dependent parameters [14–17], as reviewed by Tolias [4]. Monte Carlo approaches have also been employed to model electron–solid interactions [19,20] and applied to obtain e.g. absolute yields [21], to probe the dependence of the maximum yield on atomic number and work function [22], and to investigate the effects of surface morphology [23].

Towards the goal of a general description of SE emission, in this report the similarity between the energy dependence of the SE yield from clean materials and the log-normal distribution is examined. The measurements of Walker et al. [12] carried out in a UHV environment and at the normal angle of incidence, for carbon, iron, nickel, copper, zinc, niobium, molybdenum, silver, cadmium and tungsten are used for the analysis. These materials were found to have similar or decreased yields after cleaning, in reasonable agreement with the earlier work of Bronstein & Fraiman [8]. Additionally, the breadth of the study of Walker et al. [12], in comparison with the experiments of Shimizu [9] and Gonzalez et al. [13] where only a few materials were studied, enables the investigation of possible trends. Here and throughout, *clean* refers to samples that underwent mechanical (polishing) and chemical (isopropanol) treatment, as well as Ar^+ ion bombardment *in situ* or, in the case of Bronstein & Fraiman [8], *in situ* evaporation and cooling with liquid oxygen; *unprepared* refers to samples where no cleaning was carried out.

Following a description of existing semi-empirical models in Section 2.1, the expressions for the 3- and 4-parameter log-normal functions are given in Section 2.2 along with relationships for the maximum yields and corresponding energy in terms of the parameters. In Section 3, the results of 3- and 4-parameter log-normal fits to experimental SE yield data are shown and the goodness of fit, quantified by the

* Corresponding author.
E-mail address: g.laricchia@ucl.ac.uk (G. Laricchia).

https://doi.org/10.1016/j.nimb.2023.01.008
Received 25 April 2022; Received in revised form 12 January 2023; Accepted 15 January 2023
Available online 20 January 2023
0168-583X/© 2023 The Author(s). Published by Elsevier B.V. This is an open access article under the CC BY license (http://creativecommons.org/licenses/by/4.0/).

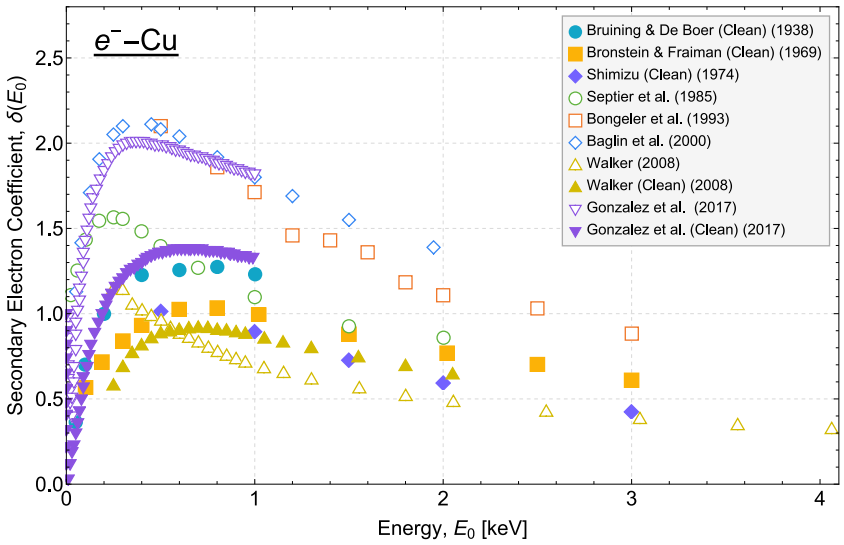

Fig. 1. Experimental data of $\delta(E_0)$ from copper for clean (filled) and unprepared (hollow) samples illustrating the discrepancies among the investigations: clean, Bruining & De Boer (1938) [7]; clean, Bronstein & Fraiman (1969) [8]; clean, Shimizu (1974) [9]; unprepared, Septier et al. (1985) [10]; unprepared, Bongeler et al. (1993) [11]; unprepared, Baglin et al. (2000) [2]; unprepared and clean, Walker et al. (2008) [12]; unprepared and clean, Gonzalez et al. (2017) [13].

coefficient of determination (R^2), is compared with those of semi-empirical models. Both log-normal functions are also fitted to the SE yield from all materials combined, normalised to the magnitude and position of the peak, and the coefficient of determination compared with previous *universal curve* models. The distributions with SE yield data from unprepared samples are also inspected. The similarity of the positron- and ion-induced SE yields to the shape of the log-normal dependence is further revealed and used to extend their energy ranges. The report is concluded with a summary in Section 4.

2. Models & methods

2.1. Semi-empirical approaches

The semi-empirical models differ in the treatment of the stopping power, $-\left[\mathrm{d}E/\mathrm{d}x\right]$, the infinitesimal energy-loss per unit depth, which is related to the yield by material-dependent parameters,

$$\delta(E_0) = -\frac{B}{\epsilon}\int_0^{R_d(E_0)} \exp\left(-\frac{x}{\lambda}\right)\left[\frac{\mathrm{d}E}{\mathrm{d}x}\right](E_0, x)\,\mathrm{d}x\,, \tag{1}$$

where B is the absorption parameter, ϵ the average energy required to liberate an electron, $R_d(E_0)$ the depth range of the primary particle and λ the characteristic SE escape length. Two forms of the stopping power are commonly employed: the generalised power law (GPL) where $\left[\mathrm{d}E/\mathrm{d}x\right] = -A/E(x)^n$ and the constant-loss model (CLM) where $\left[\mathrm{d}E/\mathrm{d}x\right] = -C/E_0^k$, with material-dependent parameters (A, C) and exponents (n, k), the latter typically in the interval $(0, 1)$.

Inserting the GPL into Eq. (1) and parametrising in terms of the maximum yield and corresponding energy (δ_m, E_m) gives [16]

$$\delta(E_0) = \delta_m \frac{G_n\left(r_m \frac{E_0}{E_m}\right)}{G_n(r_m)}\,, \tag{2}$$

where

$$G_n(r) = e^{-r^{n+1}}\int_0^r e^{y^{n+1}}\,\mathrm{d}y\,. \tag{3}$$

and r_m is the value of r for which $G_n(r)$ is maximum. The GPL of Lye & Dekker [16] and the model presented by Baroody [14] both have the form of Eq. (2) but the latter with fixed exponent $n = 1$.

Lye & Dekker [16], with insights from the experimental work of Young [24], used the CLM with $k > 0$ resulting in

$$\delta(E_0) = \delta_m \frac{H_k(z_m \frac{E_0}{E_m})}{H_k(z_m)} \tag{4}$$

where $H_k(z) = z^{-k}\left[1 - \exp(-z^{k+1})\right]$ and z_m the value of z for which it is maximum.

Furman & Pivi [17] also used the CLM but with the exponential factor in Eq. (1) replaced by $(1 + x/2\lambda)^{-2}$, yielding

$$\delta(E_0) = \delta_m \frac{\left(s\frac{E_0}{E_m}\right)}{s - 1 + \left(\frac{E_0}{E_m}\right)^s}\,, \tag{5}$$

where s is a parameter with values typically in the interval $(1, 2)$.

An alternative formulation was given by Sternglass [15] where secondary electrons are produced at a single depth determined by an approximation of the quantum-mechanical non-relativistic Bethe model [4]. In this case $\delta(E_0)$ is given by

$$\delta(E_0) = \delta_m \frac{E_0}{E_m}\exp\left(2 - 2\sqrt{\frac{E_0}{E_m}}\right)\,. \tag{6}$$

The formulae (2), (4), (5) and (6) depend on (δ_m, E_m) for each material. In addition, Eqs. (2), (4) and (5) require the parameters n, k and s respectively, determined by best-fit to experimental data.

2.2. Statistical description

Recent investigations by Laricchia et al. [25] found that the log-normal function, extensively used for the probability distribution of *macroscopic* events arising from the product of many independent random effects, may also be employed to describe the energy-dependence of inelastic collisions at the quantum level after allowing for the appropriate energy threshold, i.e. in terms of the total (or excess) energy $E' = E_0 - E_{\mathrm{th}}$ where E_0 is the incident energy and E_{th} the energy threshold.

In particular, they found that the 3-parameter function

$$f_3(E') = \frac{a}{E'}\exp\left\{-\frac{1}{2}\left[\frac{1}{b}\ln\left(\frac{E'}{x_0}\right)\right]^2\right\}\,, \tag{7}$$

could accurately reproduce the (non-resonant) cross-sections for inelastic processes (e.g. ionisation, excitation, dissociation, electron capture) by a variety of projectiles (e.g. electrons, positrons, protons, antiprotons, ions) colliding with atoms and molecules.

Laricchia et al. interpreted their result by drawing an analogy with heat capacity, considering the atom to be in thermal contact with the energy-reservoir provided by the projectile kinetic energy.

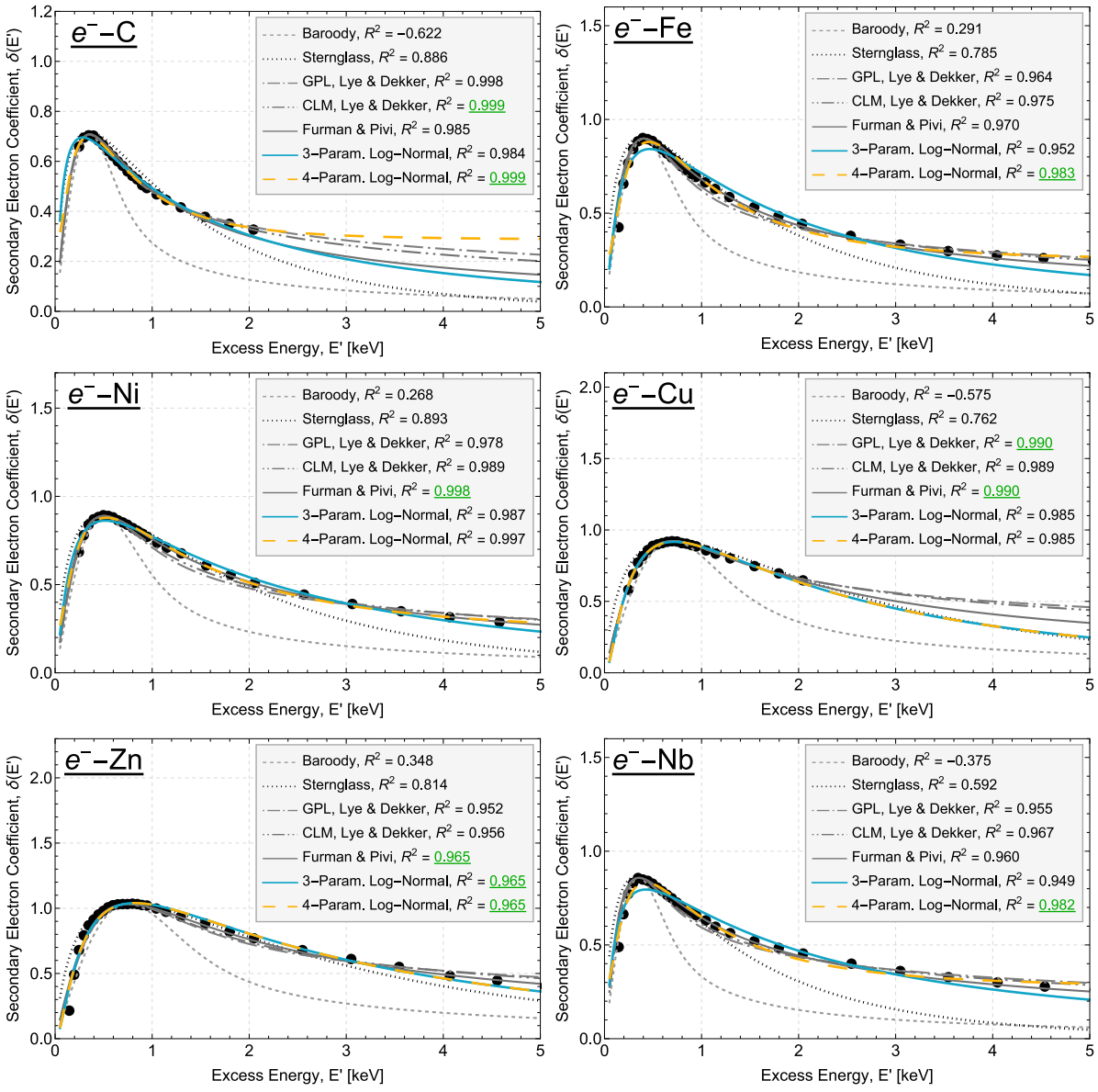

Fig. 2. Fits of $f_3(E')$ (solid) and $f_4(E')$ (long dashed) alongside experimental SE yield data of Walker [12] (symbol) for electron-impact on carbon, iron, nickel, copper, zinc, niobium, molybdenum, silver, cadmium and tungsten. Also included are the semi-empirical models of Baroody [14] (short dashed), Sternglass [15] (dotted), GPL [16] (Eq. (2), dot-dashed), CLM [16] (Eq. (4), double-dot dashed) and Furman & Pivi [17] (Eq. (5), triple-dot dashed). R^2 values are given in the legends.

The log-normal then expresses the energy-dependence of the background cross-section for a given process which proceeds through many energy-exchanges by means of virtual excitations subject to possible modulations from interference and resonance effects. The analysis was found to be general and independent from the details of the interactions at play, extending also to nuclear reactions and solid state phenomena [25].

In the present work, Eq. (7) is applied to the energy dependence of the SE yield, where E_{th} corresponds to the work function of the material (ϕ), relevant values of which are listed in Table 1. Furthermore, motivated by the investigations of Gonzalez et al. [13], who found a non-zero offset of the SE yield at low energies (< 10 eV), the 4-parameter log-normal function is also considered,

$$f_4(E') = y_0 + \frac{a}{E'} \exp\left\{ -\frac{1}{2}\left[\frac{1}{b} \ln\left(\frac{E'}{x_0} \right) \right]^2 \right\} . \tag{8}$$

The maximum of $f_3(E')$ is given by

$$f_3(E'_m) = \frac{a}{x_0} e^{b^2/2} , \tag{9}$$

and that of $f_4(E')$ is

$$f_4(E'_m) = y_0 + \frac{a}{x_0} e^{b^2/2} , \tag{10}$$

where E'_m is the position of the maximum,

$$E'_m = e^{(\ln x_0 - b^2)} . \tag{11}$$

Each set of parameters extracted from the fits of $f_3(E')$ or $f_4(E')$ are listed in Tables 2 and 3.

3. Results & discussion

The fits of $f_3(E')$ and $f_4(E')$ to the representative experimental electron-impact SE yield data of Walker et al. [12] are shown in Fig. 2 alongside those of the GPL (Eqs. (2)) and CLM (Eqs. (4) and (5)) of Lye & Dekker [16] and Furman & Pivi [17], respectively. For the comparison, the experimental data were shifted by $-\phi$ and the semi-empirical models transformed accordingly $E_0 \to E'$. The coefficient of

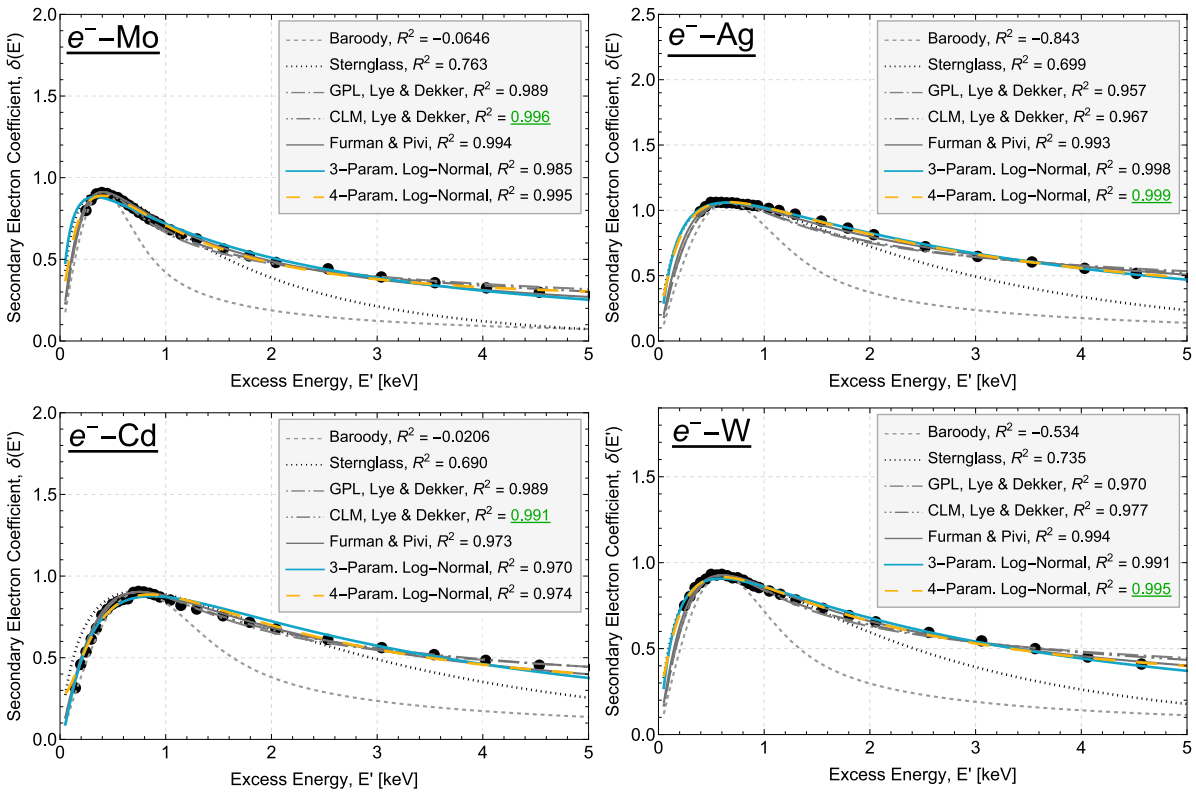

Fig. 2. (*continued*).

Table 1
Electron work functions (ϕ) of materials relevant to the current work.

Material	Work Function [eV]	Ref.
C	5.00 ± 0.10	[26]
Fe	4.50 ± 0.15	[27]
Ni	5.15 ± 0.10	[27]
Cu	4.65 ± 0.05	[27]
Zn	4.33 ± 0.10	[26]
Nb	4.30 ± 0.15	[27]
Mo	4.60 ± 0.15	[27]
Ag	4.26 ± 0.02	[27]
Cd	4.08 ± 0.02	[27]
W	4.55 ± 0.10	[26]

determination for each of the models is included in the legends, the largest value(s) for each material is shown underlined.

In all cases, the 4-parameter log-normal distribution has R^2 larger than or comparable with those of the other models, the worst instance being for cadmium where it is smaller than that of the Lye & Dekker CLM model by < 2 % (a slight step may be noted in the data for this target at $\simeq 0.7$ keV). The model of Baroody [14] underestimates $\delta(E')$ above the peak for all materials investigated. That of Sternglass [15] tends to overestimate the yield at energies below the peak and to underestimate it at higher energies except for copper, but generally to a lesser extent than the Baroody formula. In most cases, the approach of Furman & Pivi [17] yields results close to or between those from the log-normal and the GPL or CLM. The fit parameters of $f_{3,4}(E')$ for each material are listed in Table 2 together with $f_{3,4}(E'_m)$ and E'_m calculated using Eqs. (9)–(11) respectively. Parameters for $f_3(E')$ are listed instead of $f_4(E')$ where $y_0 = 0$ within errors.

When comparing the model with experimental data, Baroody commented on the existence of a *universal curve*, noticing that when normalised to (δ_m, E_m) the energy-dependent secondary electron yields from all materials follow a similar curve [14]. Equations were proposed by Lye & Dekker [16], Scholtz et al. [28] and Lin & Joy [29] to model the respective datasets. A similar analysis is carried out here by fitting $f_3(E'/E_m)$ and $f_4(E'/E_m)$ to the combined measurements of the materials in Fig. 2, with the constraints $f_3(1) = f_4(1) = 1$. The results are shown in Fig. 3 alongside the normalised data. The fit parameters of $f_4(E'/E_m)$ are stated in the inset. Also included are the fitted curves for Furman & Pivi [17], Lye & Dekker [16] and the $\log(E'/E_m)$ Gaussian form of Scholtz et al. [28] with width adjusted for best-fit ($\sigma \simeq 1.41$). The R^2 values are given in the legend.

The 4-parameter log-normal function has a larger R^2 than the 3-parameter log-normal and the model of Scholtz et al. [28]. That of the former is comparable to those of the Lye & Dekker [16] and Furman & Pivi [17] models. The combined measurements show a slight asymmetry about the position of maximum yield with a steeper decline of the reduced yield towards low energies although, at the lowest energies, the points are scarce and the scatter is large.

Fig. 4 shows $\delta(E')$ from unprepared samples of Walker et al. [12] for carbon, iron, nickel and zinc, along with fits of $f_3(E')$ and $f_4(E')$. There are large discrepancies in peak position between $f_3(E')$ and the experimental data but agreement is good towards the higher energies. The variation of the yield is followed more closely by $f_4(E')$ for carbon, iron and nickel, whereas for zinc it is almost unchanged from the $f_3(E')$ case.

In Fig. 5, application of $f_3(E')$ is extended to experimental results of SE yields from aluminium and copper induced by light-ions (H^+, H_2^+ and He^+) (Baragiola et al. [30], Hasselkamp et al. [31] and Svensson & Holmén [32]). Those for the heavier ions, Ar^+ and Xe^+, are shown in Fig. 6. All ion-impact measurements were performed in reflection geometry at the normal angle of incidence. In each figure, for a given material and projectile, the fits were determined using available data from multiple authors in combination and the coefficient of determination therefore includes the variation between datasets that are not in total agreement. The predictions have been extended over the energy range $(1 - 10^4)$ keV; the 95% prediction bands are also shown. In the case of the heavy ions, the uncertainty of the prediction rapidly increases for energies above and around the peak, due to the dearth

Table 2
Electron impact: fit parameter values (errors) of $f_{3,4}(E')$ for each material in figure 2 along with the calculated maximum yield $f_{3,4}(E'_m)$ and corresponding energy E'_m from Eqs. (10) and (11) respectively.

	a	b	x_0	y_0	E'_m [keV]	$f_{3,4}(E'_m)$
C	0.21 (0.01)	0.85 (0.02)	0.71 (0.02)	0.29 (0.01)	0.35 (0.01)	0.70 (0.02)
Fe	0.43 (0.03)	0.90 (0.04)	1.03 (0.07)	0.25 (0.02)	0.46 (0.04)	0.88 (0.06)
Ni	0.60 (0.03)	1.04 (0.03)	1.56 (0.10)	0.22 (0.02)	0.53 (0.04)	0.88 (0.06)
Cu	1.35 (0.03)	1.20 (0.02)	3.02 (0.14)	–	0.72 (0.03)	0.92 (0.05)
Zn	1.85 (0.07)	1.24 (0.03)	3.85 (0.28)	–	0.82 (0.05)	1.04 (0.09)
Nb	0.37 (0.03)	0.95 (0.05)	1.05 (0.09)	0.27 (0.02)	0.43 (0.04)	0.83 (0.07)
Mo	0.48 (0.03)	1.12 (0.05)	1.39 (0.12)	0.25 (0.02)	0.40 (0.04)	0.89 (0.07)
Ag	1.40 (0.15)	1.34 (0.05)	4.05 (0.56)	0.21 (0.04)	0.66 (0.10)	1.06 (0.16)
Cd	0.87 (0.17)	1.01 (0.09)	2.34 (0.45)	0.27 (0.06)	0.85 (0.20)	0.89 (0.18)
W	0.84 (0.10)	1.22 (0.06)	2.67 (0.38)	0.25 (0.03)	0.60 (0.09)	0.92 (0.13)

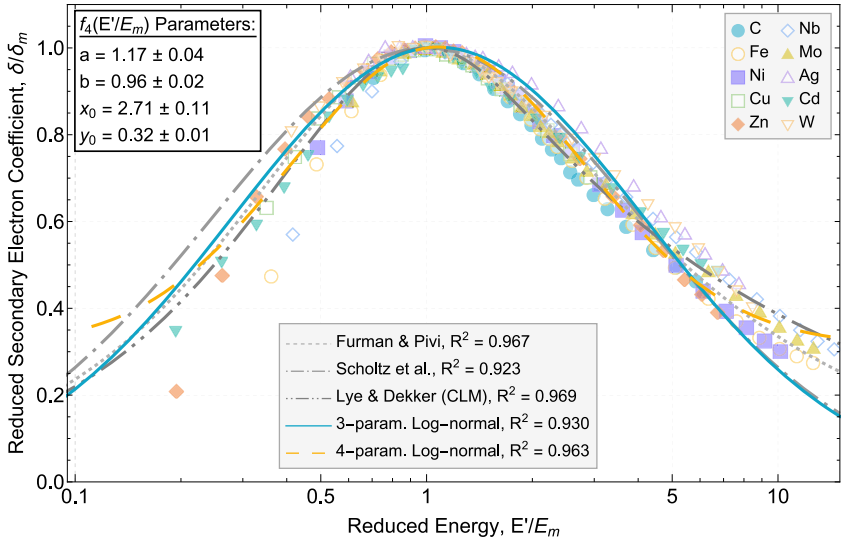

Fig. 3. Fits of $f_3(E'/E_m)$ (solid) and $f_4(E'/E_m)$ (long dashed) to the reduced experimental data of Walker et al. [12] (symbols) with the reduced energy plotted on a log-scale. Also shown are the best-fit curves for Furman & Pivi [17] (short dashed), the $\log(E'/E_m)$ Gaussian of Scholtz et al. [28] (dot-dashed) and the CLM of Lye & Dekker [16] (Eq. (4), double-dot dashed). The fit parameters of $f_4(E'/E_m)$ and the R^2 values for each curve are given in the insets.

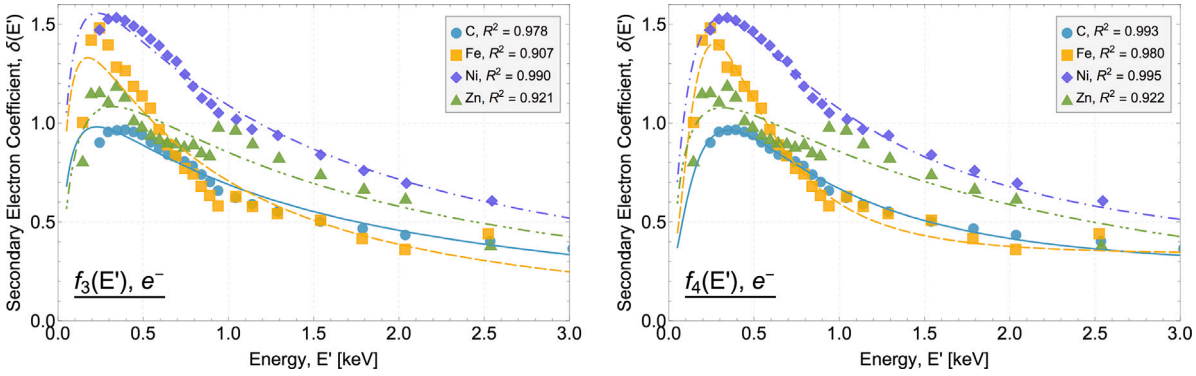

Fig. 4. Fits (lines) of $f_3(E')$ (left) and $f_4(E')$ (right) to the measurements of Walker et al. [12] (symbols) carried out prior to cleaning for carbon, iron, nickel and zinc.

of data. The values for R^2 and the log-normal parameters obtained are summarised in Table 3.

While all of the above data were acquired in the reflection geometry at normal incidence, the positron-induced SE yield displayed in Fig. 7 were obtained at different geometries and angles. In the figure, fits of $f_3(E')$ are performed to the measurements of Yang et al. [33] for carbon (4.0 μgcm^{-2} thickness in transmission geometry), and Mayer & Weiss [34] (reflection geometry) from magnesium-oxide and silicon with an incident angle of $\theta = 78^\circ$, and nickel at $\theta = 78^\circ$ and 50°. The extracted parameters and R^2 values are listed in Table 3. The variation of the yields with energy at the different geometries and angles of incidence is seen to remain consistent with the 3-parameter log-normal distribution whose predictions have been extended up to 20 keV and down to 10^{-2} keV. The plots include 95% prediction bands highlighting reasonable uncertainty beyond the range of the experimental data, even where the position and magnitude of the peak yield is not known.

4. Summary & conclusions

The 3- and 4-parameter log-normal functions expressed in terms of the excess energy ($E' = E - \phi$) were fitted to secondary electron yield measurements from clean samples of Walker et al. The R^2 values were compared with those from semi-empirical models parametrised in terms of parameters (n, k, s) and/or the position and magnitude

Table 3
Parameter values (errors) and coefficients of determination (R^2) extracted from the fits of $f_3(E')$ to the SE yield data for ion impact on aluminium and copper, and positron impact on carbon, magnesium oxide, nickel and silicon.

Target	Projectile	a	b	x_0	R^2
Al	H^+	6.63 (0.78) $\times 10^2$	1.99 (0.07)	3.70 (0.99) $\times 10^3$	0.905
	H_2^+	5.86 (0.72) $\times 10^3$	2.02 (0.05)	1.58 (0.36) $\times 10^4$	0.989
	He^+	3.67 (1.49) $\times 10^4$	2.26 (0.11)	1.35 (0.87) $\times 10^5$	0.983
	Ar^+	4.79 (4.84) $\times 10^5$	2.71 (0.18)	3.68 (5.20) $\times 10^6$	0.997
	Xe^+	1.01 (1.22) $\times 10^5$	2.24 (0.22)	3.08 (4.82) $\times 10^5$	0.997
Cu	H^+	1.19 (0.07) $\times 10^3$	1.83 (0.04)	3.49 (0.49) $\times 10^3$	0.979
	H_2^+	2.75 (1.30) $\times 10^4$	2.26 (0.15)	9.61 (7.72) $\times 10^4$	0.948
C ($\theta \simeq 0°$)	e^+	2.57 (0.11)	1.07 (0.06)	6.48 (0.56)	0.948
MgO ($\theta = 78°$)	e^+	3.11 (0.57) $\times 10$	1.71 (0.05)	1.92 (0.46) $\times 10$	0.997
Ni ($\theta = 50°$)	e^+	1.71 (0.21)	1.35 (0.06)	2.10 (0.41)	0.949
Ni ($\theta = 78°$)	e^+	6.71 (0.99)	1.50 (0.04)	8.09 (1.52)	0.997
Si ($\theta = 78°$)	e^+	9.84 (7.54) $\times 10$	2.34 (0.15)	5.89 (6.20) $\times 10^2$	0.991

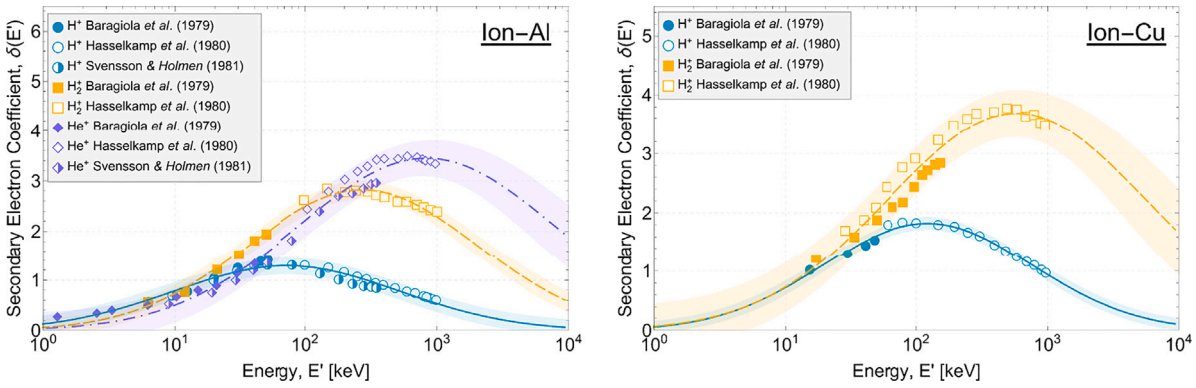

Fig. 5. Fits of $f_3(E')$ (lines) to measurements (symbols) of the ion-induced secondary electron yield of Baragiola et al. [30], Hasselkamp et al. [31] and Svensson & Holmén [32] for aluminium (left) and copper (right). Also shown are 95% prediction bands for each case.

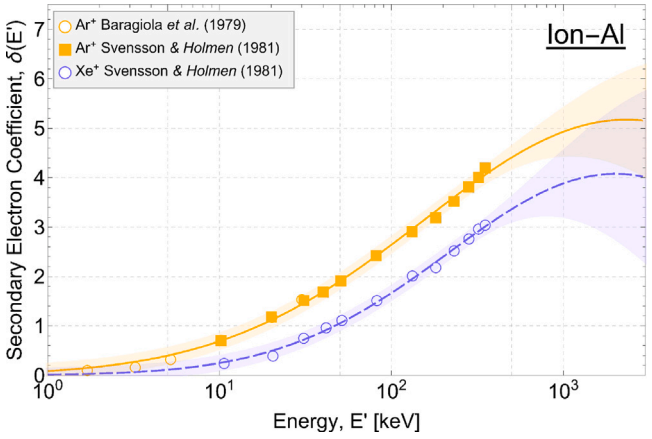

Fig. 6. Fits of $f_3(E')$ (lines) to measurements of heavy ion-induced SE yields (symbols) of Baragolia et al. [30] and Svensson & Holmén [32] from aluminium. Also shown are 95% prediction bands for each case.

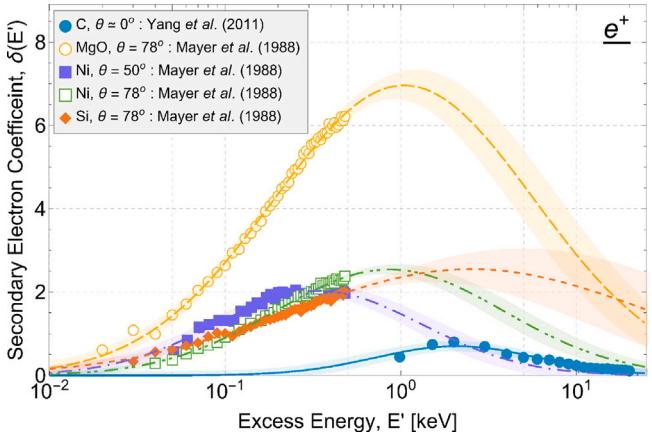

Fig. 7. Fits (lines) of $f_3(E')$ to measurements of the positron-induced SE yield (symbols) of Yang et al. [33] from carbon (4.0 μgcm^{-2} thickness in transmission geometry) and of Mayer & Weiss [34] (reflection geometry) from magnesium-oxide and silicon with an angle of incidence $\theta = 78^\circ$, and nickel with $\theta = 50^\circ$ and 78°, shown with the reduced energy on a log-scale. Also shown are 95% prediction bands for each case.

of maximum yield (δ_m, E_m). The 4-parameter log-normal distribution showed an R^2 comparable with or better than those from the other models. The secondary electron yield measurements were also considered normalised to (δ_m, E_m), and the 3- and 4-parameter log-normal distributions were fit to the combined data. Once again, the R^2 for $f_4(E'/E_m)$ has been found to be similar or greater than those of the other models. Additionally, the shape of the log-normal dependence was found to be consistent with measurements of the SE yield from unprepared samples, as well as for ion- and positron-induced SE yields, including for different geometries and angles of incidence. As illustrated for the latter projectiles, the log-normal may also be employed to extend the energy range of the SE yields even without prior knowledge of the position and magnitude of their maxima.

In conclusion, the energy dependence of the secondary electron yields by the impact of e^-, e^+ and ions have been shown to be accurately described by a log-normal distribution as a function of the excess energy E'.

In addition to its intrinsic descriptive and predictive usefulness, the present finding adds further support for the generality of the statistical

nature expressed by the log-normal function for inelastic processes at the quantum level advanced by Laricchia et al. [25].

CRediT authorship contribution statement

D.M. Newson: Methodology, Investigation, Data analysis, Writing – original draft. **R. Kadokura:** Discussion, Writing – reviewing and editing. **S.J. Brawley:** Discussion, Writing – reviewing and editing. **M. Shipman:** Discussion, Writing – reviewing and editing. **G. Laricchia:** Initiated and led the work, Supervision, Writing – reviewing and editing.

Declaration of competing interest

The authors declare that they have no known competing financial interests or personal relationships that could have appeared to influence the work reported in this paper.

Data availability

The data that support the findings of this study will be openly available at UCL Discovery.

Acknowledgements

The Engineering and Physical Sciences Research Council is gratefully acknowledged for supporting this work under grant numbers EP/P009395/1, EP/R513143/1 and for providing DMN with a research studentship. For the purpose of open access, the corresponding author has applied a Creative Commons Attribution (CC BY) licence to any Author Accepted Manuscript version arising from this submission.

The data that support the findings of this study are openly available at UCL Discovery.[1]

References

[1] H. Seiler, Secondary electron emission in the scanning electron microscope, J. Appl. Phys. 54 (11) (1983) R1–R18, http://dx.doi.org/10.1063/1.332840.
[2] B. Baglin, J. Bojko, O. Grobner, B. Henrist, N. Hilleret, C. Scheuerlein, M. Taborelli, The secondary electron yield of technical materials and its variation with surface treatments, in: Conference: EPAC 2000 : 7th European Particle Accelerator Conference, 2000, p. 217.
[3] W. Hartung, D. Asner, J. Conway, C. Dennett, S. Greenwald, J.-S. Kim, Y. Li, T. Moore, V. Omanovic, M. Palmer, C. Strohman, In-situ measurements of the secondary electron yield in an accelerator environment: Instrumentation and methods, Nucl. Instrum. Methods A 783 (1) (2015) 95–109, http://dx.doi.org/10.1016/j.nima.2015.01.092.
[4] P. Tolias, On secondary electron emission and its semi-empirical description, Plasma Phys. Control. Fusion 56 (12) (2014) 123002, http://dx.doi.org/10.1088/0741-3335/56/12/123002.
[5] S.T. Lai, Fundamentals of Spacecraft Charging: Spacecraft Interactions with Space Plasmas, Princeton University Press, 2012, http://dx.doi.org/10.2307/j.ctvcm4j2n.
[6] J. Chen, E. Louis, J. Verhoeven, R. Harmsen, C.J. Lee, M. Lubomska, M. van Kampen, W. van Schaik, F. Bijkerk, Secondary electron yield measurements of carbon covered multilayer optics, Appl. Surf. Sci. 257 (2) (2010) 354–361, http://dx.doi.org/10.1016/j.apsusc.2010.06.075.
[7] H. Bruining, J.H. De Boer, Secondary electron emission: Part I secondary electron emission of metals, Physica 5 (1) (1938) 17–30, http://dx.doi.org/10.1016/s0031-8914(38)80103-8.
[8] I.M. Bronstein, B.C. Fraiman, Vtorichnaya Elektronnaya Emissiya (Secondary Electron Emission), Nauka Publisher, Moscow, 1969, p. 340.
[9] R. Shimizu, Secondary electron yield with primary electron beam of kilo-electron-volts, J. Appl. Phys. 45 (5) (1974) 2107–2111, http://dx.doi.org/10.1063/1.1663552.
[10] A. Septier, M. Belgaroui, Secondary electron emission yields of carbon coated copper and niobium real surfaces, IEEE Trans. Electr. Insul. EI-20 (4) (1985) 725–728, http://dx.doi.org/10.1109/tei.1985.348896.
[11] R. Böngeler, U. Golla, M. Kässens, L. Reimer, B. Schindler, R. Senkel, M. Spranck, Electron-specimen interactions in low-voltage scanning electron microscopy, Scanning 15 (1) (1993) 1–18, http://dx.doi.org/10.1002/sca.4950150102.
[12] C.G.H. Walker, M.M. El-Gomati, A.M.D. Assa'd, M. Zadrazil, The secondary electron emission yield for 24 solid elements excited by primary electrons in the range 250-5000eV: A theory/experiment comparison, Scanning 30 (5) (2008) 365–380, http://dx.doi.org/10.1002/sca.20124.
[13] L.A. Gonzalez, M. Angelucci, R. Larciprete, R. Cimino, The secondary electron yield of noble metal surfaces, AIP Adv. 7 (11) (2017) 115203, http://dx.doi.org/10.1063/1.5000118.
[14] E.M. Baroody, A theory of secondary electron emission from metals, Phys. Rev. 78 (6) (1950) 780–787, http://dx.doi.org/10.1103/physrev.78.780.
[15] E.J. Sternglass, Theory of secondary electron emission by high-speed ions, Phys. Rev. 108 (1) (1957) 1–12, http://dx.doi.org/10.1103/physrev.108.1.
[16] R.G. Lye, A.J. Dekker, Theory of secondary emission, Phys. Rev. 107 (4) (1957) 977–981, http://dx.doi.org/10.1103/physrev.107.977.
[17] M. Furman, M. Pivi, Probabilistic model for the simulation of secondary electron emission, Phys. Rev. Special Top. - Accelerators and Beams 5 (12) (2002) 124404, http://dx.doi.org/10.1103/physrevstab.5.124404.
[18] D.C. Joy, A database on electron-solid interactions, Scanning 17 (5) (2006) 270–275, http://dx.doi.org/10.1002/sca.4950170501.
[19] R. Shimizu, D. Ze-Jun, Monte Carlo modelling of electron-solid interactions, Rep. Progr. Phys. 487 (1) (1992) 487–531, http://dx.doi.org/10.1088/0034-4885/55/4/002.
[20] A. Hussain, L.H. Yang, Y.B. Zou, S.F. Mao, B. Da, H.M. Li, Z.J. Ding, Monte Carlo simulation study of electron yields from compound semiconductor materials, J. Appl. Phys. 128 (1) (2020) 015305, http://dx.doi.org/10.1063/5.0012154.
[21] Z.J. Ding, H.M. Li, X.D. Tang, R. Shimizu, Monte Carlo simulation of absolute secondary electron yield of Cu, Appl. Phys. A 78 (1) (2004) 585–587, http://dx.doi.org/10.1007/s00339-002-1994-3.
[22] Z.J. Ding, X.D. Tang, R. Shimizu, Monte Carlo study of secondary electron emission, J. Appl. Phys. 89 (1) (2001) 718–726, http://dx.doi.org/10.1063/1.1331645.
[23] N. Yang, B. Song, X. Yang, R. Zhou, G. Sun, J. Xue, H. bao Mu, G.-J. Zhang, A method to numerically determine the secondary electron yield considering effects of the surface morphology, J. Appl. Phys. 130 (6) (2021) 063302, http://dx.doi.org/10.1063/5.0055542.
[24] J.R. Young, Dissipation of energy by 2.5-10 keV electrons in Al_2O_3, J Appl Phys 28 (5) (1957) 524–525, http://dx.doi.org/10.1063/1.1722794.
[25] G. Laricchia, P. Van Reeth, S.E. Fayer, S.J. Brawley, R. Kadokura, A. Loreti, M. Shipman, A statistical description of scattering at the quantum level, Sci. Rep. 8 (1) (2018) 15056, http://dx.doi.org/10.1038/s41598-018-33425-8.
[26] H.B. Michaelson, The work function of the elements and its periodicity, J. Appl. Phys. 48 (11) (1977) 4729–4733, http://dx.doi.org/10.1063/1.323539.
[27] J. Hölzl, F.K. Schulte, Work function of metals, in: Springer Tracts in Modern Physics, Springer Berlin Heidelberg, 1979, pp. 1–150, http://dx.doi.org/10.1007/bfb0048919.
[28] J.J. Scholtz, D. Dijkkamp, R.W.A. Schmitz, Secondary electron emission properties, Philips. J. Res. 50 (3–4) (1996) 375–389, http://dx.doi.org/10.1016/s0165-5817(97)84681-5.
[29] Y. Lin, D.C. Joy, A new examination of secondary electron yield data, Surf. Interface Anal. 37 (11) (2005) 895–900, http://dx.doi.org/10.1002/sia.2107.
[30] R.A. Baragiola, E.V. Alonso, J. Ferron, A. Oliva-Florio, Ion induced electron emission from clean metals, Surf. Sci. 90 (2) (1979) 240–255, http://dx.doi.org/10.1016/0039-6028(79)90341-8.
[31] D. Hasselkamp, K.G. Lang, A. Scharmann, N. Stiller, Ion induced electron emission from metal surfaces, Nucl. Instrum. Methods 180 (8) (1981) 349–356, http://dx.doi.org/10.1016/0029-554x(81)90076-8.
[32] B. Svensson, G. Holmén, Electron emission from ion-bombarded aluminum, J. Appl. Phys. 52 (11) (1981) 6928–6933, http://dx.doi.org/10.1063/1.328646.
[33] B. Yang, L.H. Cai, C.K. Ng, C.C. Ling, S. Fung, Thickness dependence of positron induced secondary electron emission in forward geometry from thin carbon foils, Nucl. Instrum. Methods Phys. Res. Sect. B Beam Interact. Mater. At. 269 (13) (2011) 1523–1526, http://dx.doi.org/10.1016/j.nimb.2011.04.107.
[34] R. Mayer, A. Weiss, Comparative study of secondary-electron emission from positron and electron bombardment of Ni, Si, and MgO, Phys. Rev. B 38 (16) (1988) 11927–11930, http://dx.doi.org/10.1103/physrevb.38.11927.

[1] https://discovery.ucl.ac.uk/id/eprint/10163263/